JOURNAL OF AIRCRAFT
Vol. 48, No. 4, July–August 2011

# Impact of Mechanical Strain Environment on Aircraft Protective Coatings and Corrosion Protection

Ung Hing Tiong* and Graham Clark†
*RMIT University, Melbourne, Victoria 3083, Australia*

DOI: 10.2514/1.C031270

**Aircraft paint schemes (paint and sealant) are a key element of corrosion preventive measures, and ensuring that such schemes and other coatings are effective and durable under service conditions is essential if corrosion costs and maintenance costs are to be minimized. Coatings can degrade under the influence of environmental factors such as exposure to moisture, high temperature, ultraviolet radiation, and so forth. Coating failure is often particularly evident at joints, and while failure may be accelerated in some regions by local variations in coating thickness and geometry at features such as edges, or by erosion, it is likely that the displacements which occur at these locations under service loads will be a contributing factor. The impact of in-service mechanical loading on coating degradation has so far received little attention, despite clear evidence that coatings tend to fail first at specific sites such as sheet ends and around fastener heads. This paper argues that the magnitude of the applied service loads and the nature of the load history should be considered in predicting and assessing rates of coating degradation, and that development of a thermomechanical history is a more appropriate approach. The likely impact of joint displacements on the protection of aging aircraft is also discussed.**

## Nomenclature

| | | |
|---|---|---|
| $a$ | = | crack length/depth, mm |
| $a_c$ | = | critical interfacial delamination length, mm |
| $D$ | = | diameter of fastener shank, mm |
| $E_c$ | = | elastic modulus of coating, MPa |
| $e$ | = | edge margin, mm |
| $G_c$ | = | critical energy release of coating, $J/m^2$ |
| $L$ | = | spacing between two perpendicular cracks in the coating, mm |
| $l^*$ | = | effective length of coating, mm |
| $K_c$ | = | critical stress intensity factor, MPa $(m)^{1/2}$ |
| $k$ | = | critical buckling stress constant |
| $t$ | = | thickness of sheet, mm |
| $t_c$ | = | thickness of coating, mm |
| $w$ | = | width of the sheet |
| $\alpha_b$ | = | initial postbuckling slope |
| $\beta$ | = | geometry factor |
| $\Delta l^*$ | = | change of effective length, mm |
| $\varepsilon_b$ | = | strain at the bottom surface of the plate |
| $\varepsilon_h$ | = | hygroscopic strain |
| $\varepsilon_m$ | = | mechanically-induced strain |
| $\varepsilon_t$ | = | strain at the top surface of the plate |
| $\varepsilon_{\text{th}}$ | = | thermally-induced strain |
| $\sigma_0$ | = | compressive residual stress, MPa |
| $\sigma_{\text{cr}}$ | = | critical tensile stress, MPa |
| $\upsilon_c$ | = | Poisson's ratio of coating |

Received 14 October 2010; accepted for publication 3 November 2010. 

*Postdoctoral Researcher, School of Aerospace, Mechanical and Manufacturing Engineering, P.O Box 71, Bundoora. In conjunction with Defence Materials and Technology Centre, Melbourne, Victoria, 3122, Australia.

†Innovation Professor, Aerospace Design, School of Aerospace, Mechanical, and Manufacturing Engineering, P.O. Box 71, Bundoora. In conjunction with Defence Materials and Technology Centre, Melbourne, Victoria, 3122, Australia; graham.clark@rmit.edu.au.

## I. Introduction

### A. Corrosion

PREVENTION and repair of corrosion is a major cost driver for both civil and military aircraft. For example, the annual direct cost of corrosion for all aircraft systems in the United States is estimated to be approximately $13 billion [1]. The Australian Defence Force has also identified corrosion as a major cause of maintenance expenditure, and manages a number of aging fleets, including F/A-18, C-130, P3-C, at bases which feature significant corrosivity. In many fleets, the traditional approach to corrosion management remains "find and fix," although the increasing use of Corrosion Prevention and Control Plans (CPCP) provides a framework for targeted inspections and treatment to help with corrosion management, and this approach is often supported by teardowns of high-life service aircraft and parts to help identify the corrosion-prone areas. When corrosion damage is detected, it is usually ground out to identify the extent of the damage, and if feasible, repaired. Unfortunately, this approach often involves time-consuming periodic inspections, lengthy maintenance processes and highly conservative "go, no-go" operational decisions, all of which are costly and may significantly impair fleet readiness. Corrosion is not yet managed effectively by design for damage tolerance [2], and if not properly controlled and managed, can impact on structural integrity by providing relatively rapid development of an initial flaw that could dramatically limit service life, and perhaps more important, could cause regions which are not usually regarded as critical to be potential failure locations. Reference [3] provides detailed descriptions of in-service corrosion commonly found in aging transport aircraft.

A proposal that corrosion should be brought more into line with other damage tolerance methodologies [4] initiated moves in the U.S. Air Force [5] to change from the find and fix approach toward a "predict and manage" philosophy, with the aim of reducing maintenance cost and increasing aircraft availability. Such a new corrosion management program requires prediction of the influence of corrosion damage on the life and residual strength of the corroded components, so that the most appropriate maintenance option can be developed.

Numerous research programs are currently underway to develop prognostic tools for the development of corrosion damage, and to improve design for reliability and maintainability. This paper describes one such program where the focus is understanding and predicting the deterioration and breakdown of protective paint coating at aircraft joints.

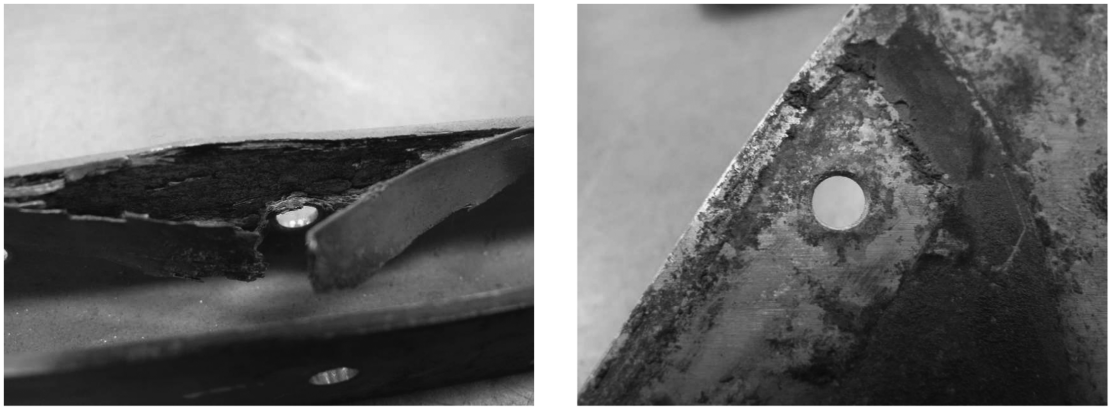

a) b)

**Fig. 1 Corrosion from a retired small aircraft, Piper Malibu JetProp: a) exfoliation at inboard pylon, and b) excessive pitting at aileron outboard hinge fitting.**

### B. Corrosion and Joints

Aircraft joints are usually key areas in terms of structural integrity, and are prone (Urban [6]) to corrosion such as pitting, exfoliation, crevice corrosion, intergranular or stress corrosion cracking, which is usually driven by the presence of moisture in the interfacial spaces between faying surfaces and between fasteners and sheet. Figure 1 shows examples of corrosion damage at the pylon and aileron on a retired small aircraft. Significantly, the corrosion damage was concentrated around the hole attachment regions, and the damage spread along the wing surface. Corrosion damage at the faying surfaces of joints can also cause pillowing or bulging of the sheets between rivets. Bellinger et al. [7] indicated that such pillowing can significantly increase stress levels in the sheet, potentially exceeding the material's yield strength. Perhaps more important, cracks associated with pillowing are very difficult to detect because current nondestructive inspection is focused on surface cracking in fatigue-critical fastener rows in joints.

The potential impact of corrosion at riveted joints attracted a great deal of attention after the Aloha Airlines accident in 1986 [8] highlighted a contribution from environmental degradation and cracking at joint faying surfaces. Visual inspection for such damage is impossible without a costly process of stripping the paint, removing rivets and opening the joints. A review by Furuta et al. [9] noted that joint specimens subjected to a corrosive environment during cyclic loading exhibited fatigue lives 30–50% shorter than those tested in an ambient environment. Further to that, studies by Hoeppner et al. [10] and Campbell and Lahey [11] both identified corrosion and fretting as significant contributing causes to both civil and military accidents for the period from the mid 1970s to 1994.

### C. Corrosion Protection at Joints

Developing and understanding ways to improve the durability of corrosion protection around joints is highly desirable in terms of ongoing management of corrosion in aging aircraft. The intrinsic corrosion resistance of alloys is insufficient to protect aircraft structural components from an aggressive environment, and protection of these metal components relies on high-quality paint coatings, acting as a barrier to the environment. Clark [12], in discussing the prediction of the effects of corrosion on structural life, noted that the prediction of overall service life of a corroded part is critically sensitive to the life of protective coatings. This is supported by several examples of in-service corrosion, given in [13], which show how the failure of protective treatments led to the initiation of corrosion. Figure 2 shows schematically the stages leading to component failure by fatigue initiating at a corrosion pit. These stages individually might be amenable to predictive modeling, and indeed a prognostic capability has been developed for fatigue cracking from pitting corrosion [14]. However, the onset of structural damage only occurs when the coating becomes ineffective, ensuring that a well-maintained durable coating is the most effective means of remaining damage-free. Since the life of coatings is critical, the development of prognostic tools for the service life of coatings, under realistic service conditions, represents an important goal which requires an understanding of the various parameters which will influence the degradation processes and rate.

### D. Aircraft Paint Coatings

A typical military paint coating will have three layers [15], namely a polyurethane topcoat ($\sim$20 $\mu$m), an inhibited epoxy primer ($\sim$25 $\mu$m ), and a chromium conversion coating ($\sim$0.1–0.2 $\mu$m ) or thicker ($\sim$1–5 $\mu$m) anodized coating, see Fig. 3. The internal paint scheme is usually primer-only with extensive use of sealants in some areas. Each layer in the coating system has one or more roles; the topcoat layer provides appearance and protection against environmental erosion and mechanical abrasion, as well as retarding moisture ingress, while the surface chromate (or similar) treatment layer provides passivation of the metal surface, optimizes topography for primer adhesion, and inhibits corrosion. In addition to that, a sealant such as polysulfide sealing compound or zinc chromate primer is often applied at faying surfaces, exposed sheet ends and around fastener holes; sealants prevent penetration of joints by the environment or fuels, and maintain flexibility of the coating system. Current aircraft coating schemes have been subjected to extensive refinement, and if correctly applied, perform well. Ideally they will last for 6–8 years in service.

The topcoat is extremely sensitive to ultraviolet degradation, causing chalking or discoloration, hence refinishing may be required after as little as 18–24 months. It can also display mechanical damage such as scratches, and repair or refinishing can introduce nonuniform external surface features which like scratches can act as crack

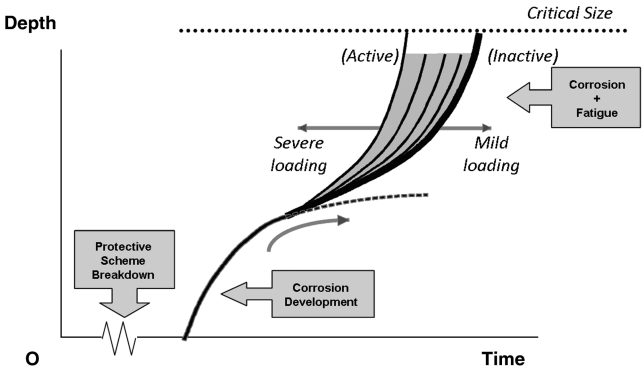


**Fig. 2 Schematic of stages in failure of a corroded part by fatigue crack growth initiating at corrosion [12].**

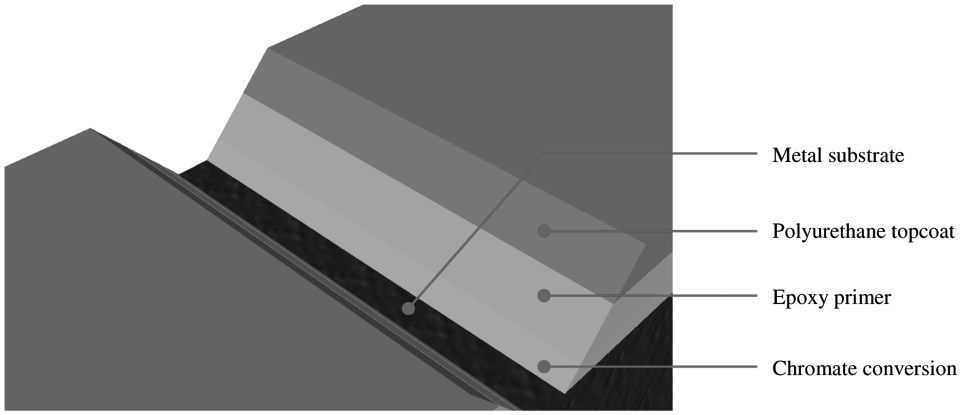


**Fig. 3 Typical aircraft coating system which consists of topcoat, primer, conversion coating, and the underlying metal.**

initiation points. The first visible sign of paint failure is usually cracking of the (typically topcoat) layer [16]; this may cause functional failure of the coating and indirectly promote component failure through corrosion and/or cracking. As an example, cracking of paint around a fastener head (see Fig. 4 which illustrates such paint cracking in a retired military aircraft wing panel) can allow moisture to penetrate into the interface underneath the fastener head and subsequently initiate corrosion.

Other studies [13,17] also revealed the coatings tend to crack or blister around fasteners under cyclic flight loads and repeated exposure to a temperature range of −54–163 °C. An example given in [13] identified two factors, cracking of the polyurethane finish and the absence of sealant between the fasteners and countersink, that were believed to play a crucial role in the development of exfoliation corrosion adjacent to fasteners on the external wing surface of a fast jet. To improve corrosion resistance around the fastener area, it is common to install fasteners wet with inhibited polysulfide sealant which gives an increased tolerance to flexing [17].

The National Materials Advisory Board (NMAB) in its Aging U.S. Air Force Aircraft final report [18] noted that aircraft coatings need to meet a demanding set of criteria (Recommendation 18), including 1) ambient curing, 2) long-term corrosion protection and adhesion to a wide variety of substrate, 3) resistance to environmental chemical exposure (e.g., hydraulic fluids, fuels, solvents, cleaning solutions), 4) long-term exterior durability with minimal change in optical or physical properties, and 5) mechanical durability to operating stresses and in a fretting environment.

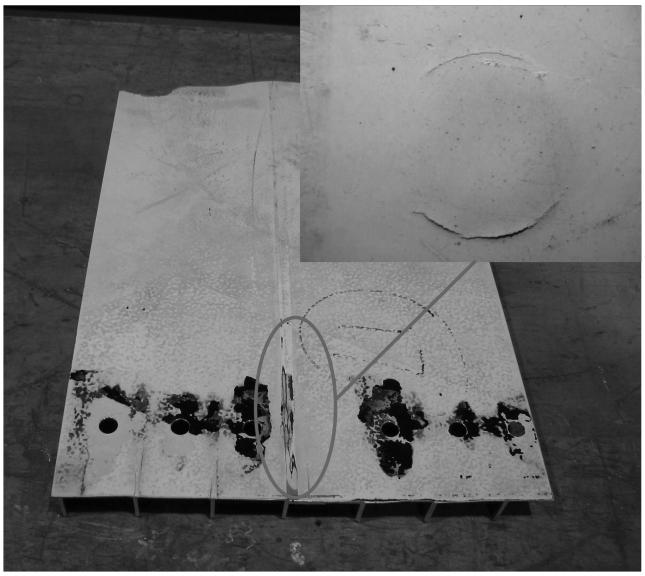

**Fig. 4 Cracking of protective coatings around fastener head (insert) in a retired military aircraft wing skin [68].**

The present work addresses the issue raised in the NMAB (point 5) and forms part of a larger research program which is developing tools for predicting the impact of real service environment on coating longevity for military aircraft in Australia. The benefits of such a prognostic capability include:

1) An ability to predict the degradation and failure of coatings under realistic flight conditions.

2) Tools to allow prediction of the regions where coatings degrade rapidly, allowing preventative maintenance or restoration of the coatings.

This paper identifies and describes the key features of the mechanical loading at aircraft joints which might affect coating longevity. The specific aim was to identify, predict and measure the joint displacements at locations where coatings might experience localized strain in service. The results of this work will contribute to development of a more comprehensive and realistic picture of the thermomechanical environment which is applied to coatings throughout service life. Understanding that environment will ultimately assist with evaluation and development of protective coatings, prediction of degradation rates to allow improved maintenance, and identification of key coating failure locations so that they can be managed more effectively. All these research efforts are aimed at incremental improvements in corrosion prevention and in-service management that may potentially save millions of dollars of corrosion-associated maintenance expenditure.

## II. Background

### A. Aircraft Joints and Loading

The performance of mechanically fastened joints under an aircraft service environment is complicated by many issues which can affect the durability of the joint; these include preload/clamping forces, the effect of variations in frictional load transfer at faying surfaces, out-of-plane bending (secondary bending and applied bending), size of fastener hole, and hole interface clearance, [19]. Many of these factors are interrelated, since, for example, fastener torque and overall clamping force will affect the amount of frictional load transfer through the faying surfaces, and the way in which these factors collectively affect joint degradation means that accurate prediction of joint service life remains a formidable challenge. Joints usually represent weak links in the structure, because of high localized stresses and stress redistribution at the fastener locations, and the majority of critical locations for structural failure occur at or near joints and splices. As a result, joint locations absorb substantial time and effort in terms of design, inspection and maintenance.

Mechanically fastened joints transfer applied load from one structural member to another via fastener shear and also through friction through the faying surface. Each fastener row in different joint configurations carries a different amount of applied load [20,21]. Starikov [22] reported that the load transferred by friction forces increased substantially during fatigue loading due to fretting wear on the faying surfaces; in his joints 80–90% of the applied load was carried by friction and the rest was transferred by the fastener

shear, highlighting the significance of the friction forces in the load transfer at joints.[‡] This view is supported elsewhere [23–26]. However in other studies [22–25], friction was shown to be a minor factor which may be neglected. Tate [27] suggested that friction may be significant only when clamping forces are high, implying that loss of clamping pressure can lead to increased fastener bending and early fastener failure.

The complex mechanism of load transfer combined with the stress concentration due to holes and deformations from secondary bending gives rise to a complex three-dimensional stress distribution around holes, and this is of prime importance because fatigue cracks often initiate in service at or near the fastener hole [28,29]. Several factors influence the stress distribution, as reported by Eastaugh et al. [28], these include clamping force applied by the fastener, surface shear within the clamping zone of the fastener due to load transfer through friction, pin-loading at the hole due to load transfer through fastener shear, and internal pressure in the hole due to expansion of the fastener. A number of parameters guide design of mechanical joints. Sharp et al. [30], Niu [31], and Park and Grandt [32] present thorough descriptions and the following sections summarize some of the key factors:

1) Common failure modes for mechanically fastened joints, namely fastener shear failure, sheet tension failure, sheet bearing failure and sheet tear out failure, are illustrated schematically in Fig. 5.

2) The fatigue strength of mechanical joints is strongly affected by fastener arrangement. As fastener pitch increases, the fatigue strength of a joint deteriorates due to an increase in the stress concentration at each fastener. The fastener pitch (center to center) is recommended to be between $4D$ to $8D$.

3) Countersunk fasteners are normally used on the exterior of aircraft to minimize drag. The depth of countersink should be less than two thirds of the skin thickness to avoid high stress concentration due to development of a "knife-edge" geometry.

4) Interference-fit fasteners are used widely to improve the fatigue performance of fastened joints. The interference should be at least 1% of the fastener diameter for optimal results.

5) Joint configuration also has a significant impact on fatigue strength. Single lap joints tend to bend during fatigue loading as a consequence of eccentricities in the joint.

The applied loading has a significant effect on local stresses and deflection of the joints and is an important consideration in the work described in this paper. Several points are worth highlighting:

1) Ideally, the joint will be loaded longitudinally, although the overall structure may feature significant bending deflection and that may be reflected in localized bending applied to the joint.

2) A more common source of applied bending is fuselage pressurization, which provides significant out-of-plane bending where the skin attaches to the stiffer supporting frames.

3) Another form of out-of-plane bending, more commonly known as secondary bending, is a result of the inherent eccentricity caused by the offset of the load line from the neutral axis of the joint members where the load is transferred between members. This causes bending deflection and results in nonuniform stress distribution through the thickness of the sheets [33]. Finney and Evans [34], on the basis on their strain gauging survey of 150 aircraft, showed that 85% of them exhibited secondary bending. High levels of secondary bending have detrimental effects on fatigue durability of the joints [34], amplifying the stress concentration of fastener holes and load transfer by the fasteners. Thus, it is desirable to minimize the effects of secondary bending in the design of joint details, to the extent that a specimen with excessive bending would not be representative of typical aircraft joint [32]. Schijve et al. [33] have proposed the neutral line model to analytically analyze the structural significance of secondary bending. Eastaugh et al. [28] showed that the bending stress is greatest along a line roughly tangential to the fastener holes, where the bending ratio, given as $(\varepsilon_b - \varepsilon_t)/(\varepsilon_b + \varepsilon_t)$, was measured as 0.45. Note the subscript $b$ and $t$ denotes the bottom and top surfaces of the skin. Schutz and Lowak [35] showed that, on an actual fuselage splice, the bending ratio typically ranges from 0.2 to 1.8.

Unfortunately, the effect of secondary bending has received little attention in the literature and is often ignored in the fatigue analysis of mechanically fastened joints [33]. The research discussed in this paper includes this factor, and its impact on joint sheet end deflection, and therefore on the coating performance.

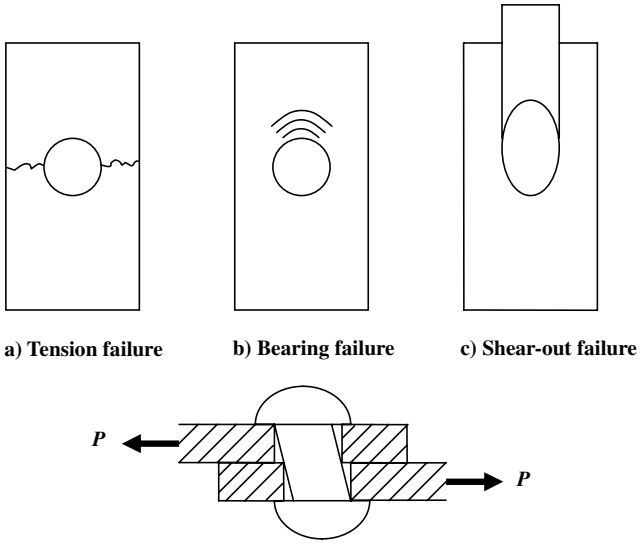


**Fig. 5 Common failure modes of mechanically fastened joints [30].**

### B. Coating Failure Environment

The durability of coatings has been studied extensively, and the rate of coating degradation is found to be influenced by several environmental factors. Under outdoor weathering exposure, ultraviolet radiation (UV) exposure and the combined function of heat and moisture (hydrothermal effects) are the two most critical factors contributing to degradation [32–37]. In the present study, the coating degradation due to UV is a prime concern for polyurethane topcoat, but has little effect to its underlying epoxy primer, because this layer is never normally exposed to UV. Nevertheless, hydrothermal degradation has detrimental effects on both topcoat and primer, and thermal radiation has been found to penetrate the topcoat and degrade the underlying primer [36].

Degradation of polyurethane topcoats can be observed by changes in appearance and mechanical properties (i.e., tensile strength, elongation, impact strength and elastic modulus); common effects are discoloration, embrittlement, tackiness, loss of surface gloss, crazing or chalking of the surface [37]. Ranby and Rabek [38] reported that in the presence of UV and oxygen, polyurethane topcoat undergoes a photo-oxidation process, which is accelerated by the presence of water. This is often followed by loss in mechanical and physical properties. For instance, Skaja et al. [39], Kramb et al. [40] and Guo et al. [41] observed a significant increase in elastic modulus on the coating surface which was suggested to be related to the formation of oxidative products. Skaja et al. [39] found physical aging of the polymer network occurred concurrently with photo-oxidation which caused the modulus increase. Other studies by Bondzic et al. [42] also highlighted the role of high temperature in contributing to coating degradation as it can increase the rate of photo-oxidation; Thompson et al. [43] showed that hydrolysis can cause chain scission in polyurethane topcoat, leading inevitably to deterioration in coating properties.

Yang et al. [44] monitored the degradation of polyurethane topcoat in an accelerated weathering test chamber and noted the formation of blisters on the coating surface during the early stage of degradation process; the blisters increased in concentration and size with longer

[‡]The specimens were metallic: different conditions prevail in composite-to-composite and composite-to-metallic joints.

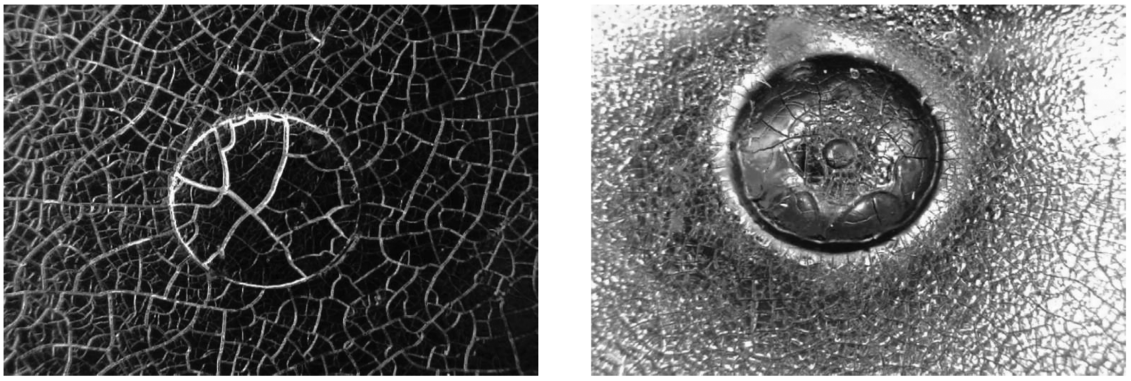

**Fig. 6 Common failure modes for thin coatings: a) cracking (under tensile stress), and b) interfacial buckling delamination followed by spalling (under compressive stress).**

UV exposure time, and subsequent micro-cracking and loss of coating gloss occurred as a result of local blister breakage [45]. In other work specifically on aerospace coatings, Tangestanian et al. [46] studied the effect of aging on the physical properties (e.g., hardness and modulus of elasticity); AA2024-T3 panels painted with polyurethane and artificially aged at 100°C showed increased static and dynamic hardness of the coatings while aging did not have a significant effect on the modulus of elasticity. In addition the aging process made the coating more erosion resistant.

The influence of stress concentrations on the rate of photo-oxidation reaction in a much wider range of polymers has been reviewed by White and Turnbull [47], Terselius et al. [48] and Popov et al. [49]. In many practical applications the coating layers are stressed by internal residual stresses (due to internal chemical reactions such as oxidation [49], deposition processes or thermal transients) or by externally applied loads; these stresses can alter the effective activation energy for a photo-oxidation reaction, and subsequently affect the rate of degradation [50].

In contrast to research on chemical and physical aging/degradation of polyurethane coatings, the role of mechanical stress, and especially the loading/strain *history*, as a contributory part of the overall environmental coating degradation model has received little attention. The loading history is likely to interact with the other aging processes, and may also play a role in the ability of the paint to tolerate mechanical damage; a slight scratch may be all that is required to diminish coating durability, and the applied loading is likely to influence the progress of such damage.

The mechanical environment applied to an aircraft coating is strongly influenced by geometric constraints, service stresses and thermal gradients. Under these in-service conditions, the coating layer may contract, elongate or bend, leading to coating failure. Figure 6 illustrates two of the most common failure modes of coatings, i.e., 1) cracks which progress through the thickness and/or 2) cracking along (or parallel) the interface between coating and metal substrate [51]. Most of this cracking is assumed to initiate from preexisting defects, voids or surface scratches (which are presumably more common on the surface) and with sufficient initiators, isotropic stressing (e.g., thermal stressing) will result in "mud-flat" crack networks, see Fig. 7.

Assuming linear elastic behavior of the coating/substrate system, surface cracks, subjected under tensile stress, will fracture perpendicular to the interface when the in-plane stress exceeds a critical stress value $\sigma_{\text{cr}}$ [51]:

$$\sigma_{\text{cr}} = \frac{K_c}{\beta\sqrt{\pi a}} = \sqrt{\frac{E_c G_c}{\beta^2 \pi a}} = \frac{E_c \varepsilon_{cr}}{(1-\upsilon_c)} \tag{1}$$

where $K_C$ is the critical stress intensity factor of the coating, $\beta$ is geometry factor, $E_c$ is the Young's modulus of the coating system, $G_c$ is the critical energy release rate, $\varepsilon_{\text{cr}}$ is critical strain at failure (or elongation-at-break), $\upsilon_c$ is Poisson's ratio of coating, and $a$ is the crack size. A critical strain (such as elongation-at-yield or elongation-at-break) is more commonly used to describe the fracture criterion for tensile cracking in the coating, rather than critical stress. Comprehensive reviews by Strawbridge and Evans [51] noted that it has been observed that the through-thickness cracking in the coating could also cause crack propagation into the metal substrate, or interface decohesion.

One of the aspects worth noting is the spacing of the cracks, $L$ (see Fig. 6a), which tends to be uniform due to the development of the maximum shear stress at the midpoint between the coating segment between two existing surface cracks [52]; as a result, there is a propensity for formation of new cracks at or near these midlocations once the stress level exceeds the value of $\sigma_{\text{cr}}$. One experimental approach in research into multiple cracking is to count the number of coating cracks as a function of applied load [53].

Under compressive loads, coatings can fail by cracking at the coating interface followed by buckling and eventually spalling [54], and this is exacerbated by weak interfacial bonding. Thouless [55] and Hutchinson et al. [56] explicitly commented that buckling delamination is often observed to occur above an intrinsic defect under compressive residual stress, as well as at locations where there is an initial flaw in the interface between film and substrate. Buckling can occur when the compressive stress exceeds the critical value $\sigma_b$ [57]:

$$\sigma_b = \frac{kE_c}{12(1-\upsilon_c^2)}\left(\frac{t_c}{a}\right)^2 \tag{2}$$

where $k$ is approximately 14.7 (constant), $t_c$ is the coating thickness and $a$ is the length of the preexisting interfacial crack (void). According to Hutchinson et al. [56], after coating buckling has initiated, the delamination will propagate only when it exceeds the critical interfacial delamination length $a_c$, i.e., approximately 20 times the thickness of the coating or more for typical moduli and film/coating compression levels. This critical interfacial delamination length can be expressed as [54]:

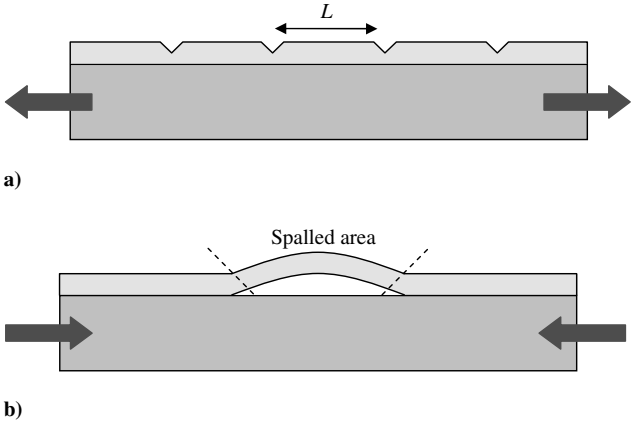


**Fig. 7 "Mud-flat" cracking around fastener heads.**

$$a_c = \left(\frac{K_c}{\sigma_0}\right)^2 \left(\frac{kE_c}{\sigma_0}\right) \left[\frac{3}{4(1-\alpha_b)} \sqrt{\frac{1+\upsilon_c}{1-\upsilon_c}}\right] \tag{3}$$

where $K_c$ is the critical interfacial fracture toughness, $\sigma_0$ is the compressive residual stress and $\alpha_b$ is the initial postbuckling slope, given as:

$$\alpha_b = \frac{1}{1 + 1.207(1+\upsilon_c)} \tag{4}$$

Another failure mode can occur under compressive stress, as noted by Evans and Lobb [58]. When interfacial bonding between the coating and substrate is strong, compressive shear cracking of the coating can occur first, probably initiating from a preexisting defect. This would produce spallation of the segment bounded by the shear cracks by means of wedging.

Under repeated cyclic loading (seen by the coating as a combination of tensile and compressive applied loading), mechanically fastened joints can exhibit substantial displacements, and these displacements, if large enough, can influence and promote cracking in the overlying coatings, allowing moisture penetration. In the following sections we discuss the strains likely to be experienced by a coating as a result of applied mechanical strain using two aircraft joint geometries.

## III. Joint Features and Selection of Locations

Although aircraft joints are often complex, they can generally be modeled as simple configurations, with one or more rows of fasteners. The simple lap joint has two sheets that are lapped over each other and fastened together by one or more rows of fasteners, while in a butt joint, the edges of two sheets are butted together, with the sheets connected by a joining member (a cover plate, or underlying structure).

Joints experience displacement as a result of applied loading and thermomechanical cycling, with the joint effectively concentrating the remotely applied strain into discrete locations. This is shown in Fig. 8 which highlights potential locations where the local strain effects might be expected to influence coatings, and more specifically, to influence coating longevity [59,60]. The regions illustrated are those where there is an observed propensity for coating cracking around sheet or butt ends, and fastener heads. These locations, in practice, often require regular inspections and if damage is detected, this may be followed by repair or reapplication of the protective coating.

Essentially there are two joint movements of concern. These are:

1) Shear displacement of the joint members which affects faying surface interfaces, and leads to displacements at sheet ends. It also leads to movement of hole surfaces such as countersinks and bores, and therefore may lead to fastener rotation and issues such as bearing failure and fretting. Although the shear movements are relatively small (usually submillimeter) the small regions in which they are concentrated could lead to substantial strains in an overlying coating.

2) Rotational displacements of the joint due to applied bending loads, or arising from load line eccentricity (commonly known as secondary bending).

A variety of fastener types are used in aircraft and the present study will focus on two common variants: countersunk and domehead fasteners, applied here in a two-row simple lap joint. Each of these two joint designs possesses its own unique fatigue strength, which is a function of materials used (both sheets and fasteners), and fastener arrangement [30].

## IV. Displacement Analysis

### A. Lap Joint (Countersunk)

Countersunk fasteners are commonly used on the exterior of aircraft to maintain aerodynamic performance (minimizing drag). If the countersink depth is similar to the sheet thickness, it can produce

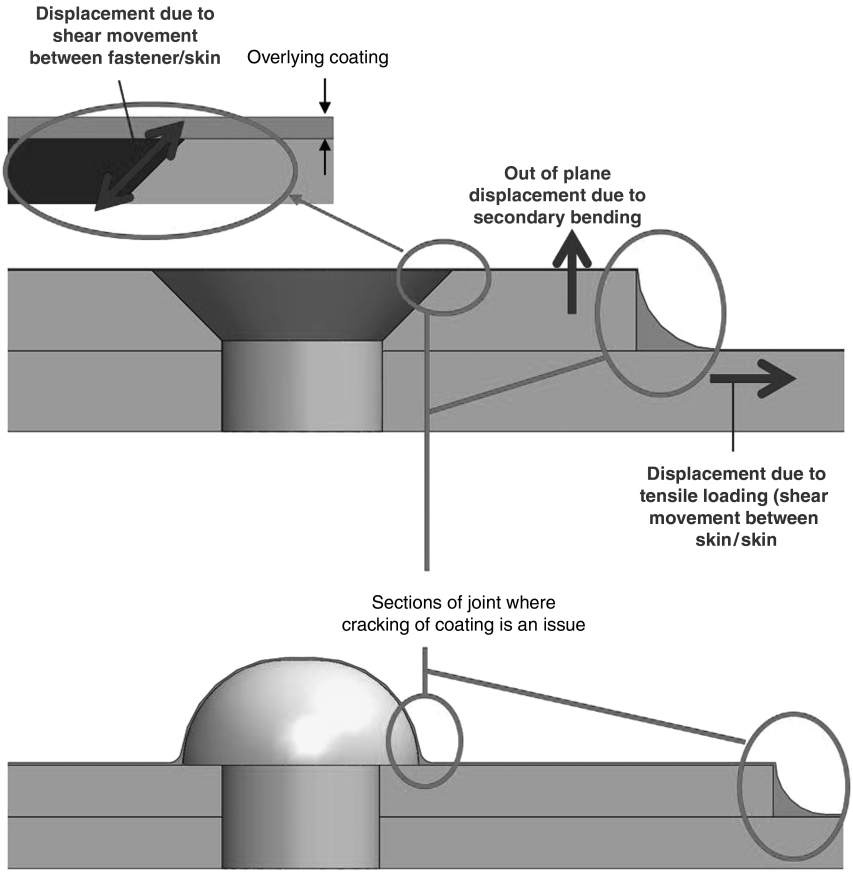


**Fig. 8 Schematic of typical shear interface in mechanically fastened joints [59].**

a "knife-edge" condition which could cause fatigue cracking in aircraft structures. As a result, it is common to recommend that the thickness of the top (countersunk) sheet be at least 1.5 times the depth of the countersink.

Starikov [22] described three sets of fatigue experiments conducted on mechanically fastened joints subjected to the FALSTAFF (fighter aircraft loading standard for fatigue evaluation) spectrum, and discussed numerous parameters that influenced the fatigue performance of joints. These included secondary bending, load transfer between bolts, and frictional wear. The present study is based on a finite element model constructed using COSMOSWorks, and the initial step used the joint configuration and strain distributions obtained from Starikov [22] to validate the analysis. The geometry is a lap joint test specimen (see Fig. 9) with two $50 \times 200$ mm aluminum alloy AA7475-T761 sheets 3 mm thick, fastened together using four countersunk fasteners. The area of faying surface is $50 \times 50$ mm$^2$. The fasteners are made from Ti-6Al-4V with a shank diameter of 6 mm and are installed with an interference fit of 50 micrometers using Hi-Lok nuts.

The critical failure stress of this joint is calculated to be 191 MPa (corresponding to sheet tension failure) based upon the joint design allowable stresses of four possible failure modes, given in Fig. 5. It is worth nothing that the applied loading used in this analysis is high. In normal operating conditions, a joint should not normally experience more than about $2/3$ of this extreme value [60].

### B. Generic Lap Joint (Dome-Head)

Another joint configuration considered in this study consists of two 57.15 mm (or 2.25 in.) $\times$ 134.62 mm (or 5.3 in.) aluminum alloy AA2024-T3 bare sheets with a thickness of 1.016 mm (or 0.04 in.), see Fig. 10. The sheets are lapped by 38.1 mm and fastened together with two parallel rows of three fasteners (MS20470AD4-6 domehead, made from 2117-T4 (AD) material with a shank diameter of 3.175 mm). The edge distance perpendicular to the loading direction is 9.53 mm while the fastener pitch is 19.05 mm (or 0.125 in.). In terms of skin thickness, fastener type and fastener spacing, this joint is a simple representation of many found in light (General Aviation) aircraft. To contain the number of variables in the analysis, the joint is initially assumed to be unsupported, i.e., no underlying structural attachment is considered in this initial analysis. The presence of such substructure would add an additional variable in the form of joint eccentricity.

The joint has a critical failure stress of 169 MPa (corresponding to fastener shear failure). This value was used in the finite element analysis, acknowledging that it is higher than service stressing.

## V. Modeling Techniques and Validation

### A. Finite Element Modeling

The validity of the finite element model was evaluated by comparing the predicted strain distributions to those measured experimentally. Use was made of experimental data of Starikov [22], and the specimen configuration in Fig. 9 was chosen for this purpose. Taking advantage of symmetry, the analysis was performed on a half-lap joint model only. The finite element model, of 101,684 nodes and 63,750 elements, was generated using COSMOSWorks with 10-noded tetrahedral elements. A tension applied load giving 150 MPa was applied on two end surfaces of the model while the minimum applied stress is given as $-39$ MPa.

The top and bottom surfaces of the sheets were modeled constrained from out-of-plane deformation, to simulate the use of an antibuckling fixture as adopted in the test [22]. These two sheets are joined with two countersunk fasteners via a connect mechanism function known as bolt connector, available in the FE software which allows users to define the interaction between the sheets and fasteners in a single operation rather than having to create a series of constraints. The preload axial force was approximated as 7.91 Nm (assuming a torque coefficient of 0.2). This is an average value between the figures of 6.78–9.04 Nm recommended by Hi-Shear Corporation [61].

Surface interactions were defined using a contact mechanism in the software known as *no penetration*; these contact relationships are applied on the faying surfaces between the fasteners and sheets, and between the upper and lower sheets. A coefficient of friction of 0.2, for generic joints [22,62], was specified for all faying surfaces.

### B. Strain Gauges

Starikov employed strain gauges in numerous specimen locations [22]; Fig. 11 shows the location of some of these gauges, i.e., between two fastener rows, 27.5 mm from the edge of sheet ends. The distance between two strain gauges was approximately 6.25 mm.

### C. Validation Results

Figure 12 shows the equivalent strain distributions at the strain gauge location (along the width of specimen) predicted using the finite element method. These values are compared in Fig. 13 with the experimentally measured values, and are shown as a function of the strain gauge positions relative to the joint width, $w$, where $w = 0$ corresponds to the side edge of the joint sheet. The tension and compressive applied load peaks are shown by filled diamond and triangle symbols, respectively. From the finite element results, the strain maxima are observed at the sheet edge ($w = 0$ mm) and in the

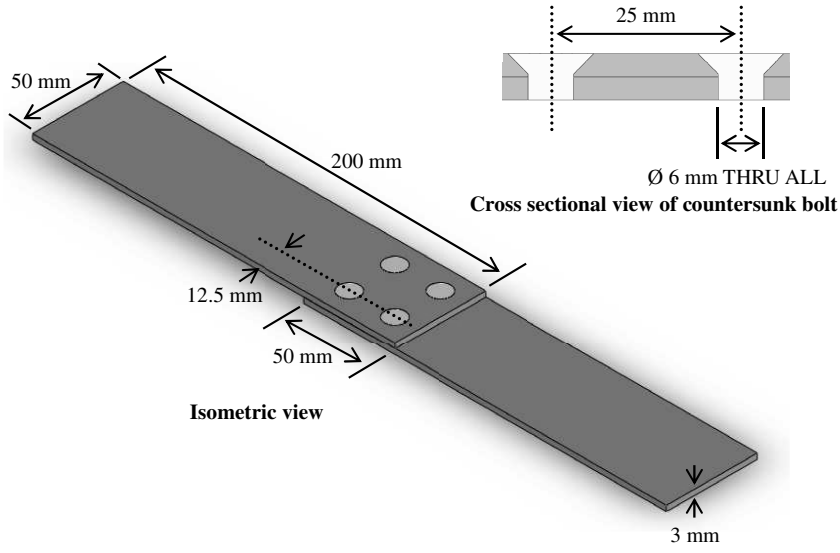


**Fig. 9 Geometry of lap joint specimen (countersunk).**

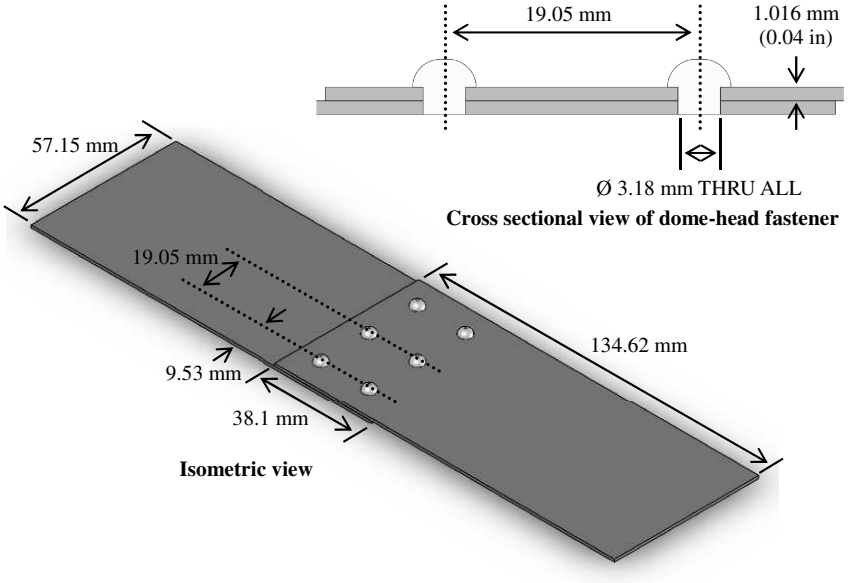


**Fig. 10 Geometry of generic lap joint specimen (domehead).**


**Fig. 11 Location of strain gauges [22].**

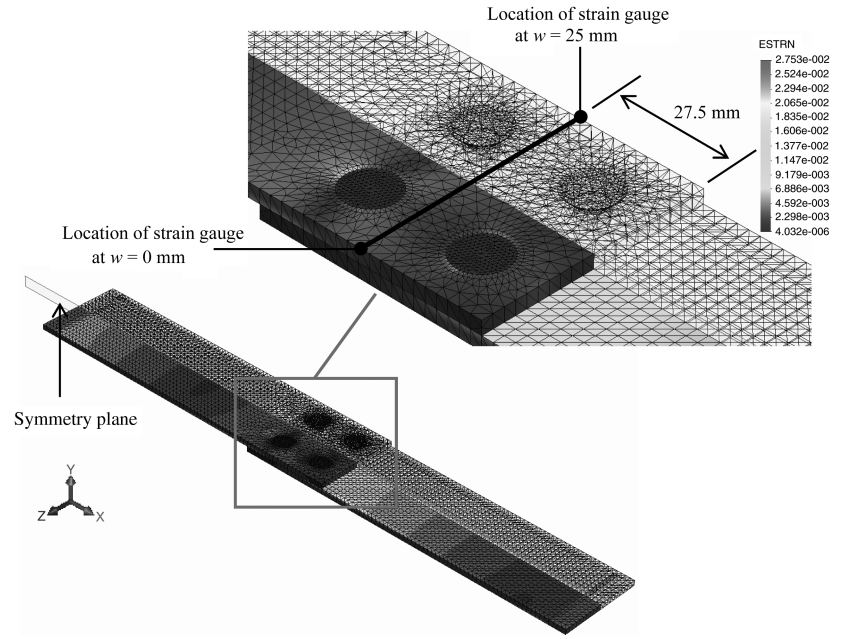


**Fig. 12 Equivalent strain distribution of a loaded simple lap joint (countersunk).**

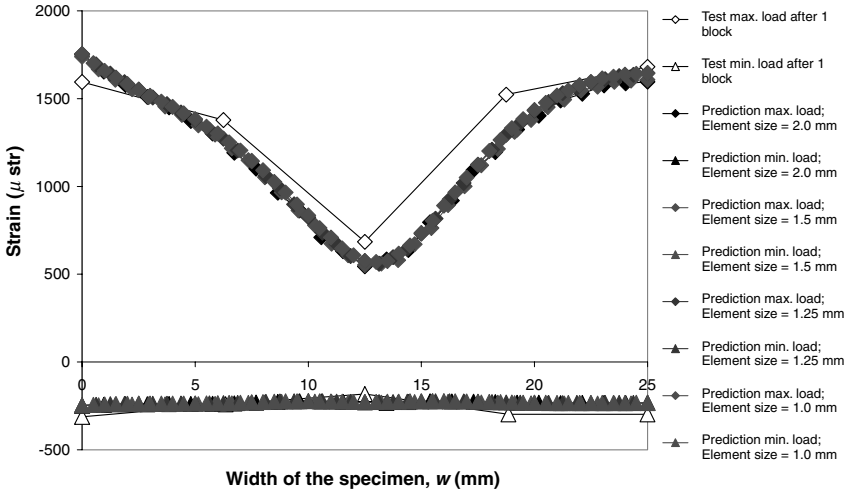


**Fig. 13 Strain distributions between two fastener rows.**

middle of the joint sheet ($w = 25$ mm), while the strain minimum is predicted at a location between two fasteners, i.e., $w = 12.5$ mm. Overall, the initial predicted strain distribution curves across the width of the specimen correlated moderately well with the test results for both tensile and compressive applied loads.

Of particular interest is the strain behavior at $w = 12.5$ mm where the strain minimum at this location is dominated by the influence of two fasteners. Mesh sensitivity studies were undertaken to examine the effects of mesh size on the accuracy of the strain prediction at $w = 12.5$. Tables 1 and 2 show the summary of predicted strain values with respect to different element sizes (mesh density). The model was run a number of times with four different element sizes, i.e., 2, 1.5, 1.25, and 1 mm. While the initial run used an element size of 2 mm, yielding 20.4% (tension) and 25.9% (compressive) differences between the predicted and measured strain values at $w = 12.5$ mm, both Table 1 (for tensile load cases) and Table 2 (for compressive load cases) show an improvement in strain correlation as the element size deceased. An element size of 1.25 mm was adopted since it produced the optimum strain correlation in the element size sensitivity study, with an acceptable computational run time. Having made this refinement, a second validation was carried out to study the influence of applied stresses on strain behavior at the location between two fasteners ($w = 12.5$ mm), as well as at the middle of the joint sheet ($w = 25$ mm).

Figure 14 shows that the finite element predictions agreed reasonably well with the stress-strain measurements from Starikov [22]. This was particularly true for stress-strain prediction at the middle of the sheet ($w = 25$ mm) where a linear behavior was observed. As for the stress-strain relationship between the two fasteners (at $w = 12.5$ mm), the measured strain increases linearly as the applied stress increases up to 40 MPa. However from this point some nonlinear behavior was observed. This is believed to relate to contact forces between the fasteners and sheets causing compressive deformation in the region between two fasteners [21,63], and thus affecting the strain gauge measurements and measured strain distributions. Further to that, it is speculated that, at lower applied stress range, the transferred loads are not equally distributed between two fasteners, with one experiencing higher transferred load than the other. As such, lower strains are transmitted across the region between two fasteners. As a result, as can be seen in Fig. 14, the finite element analysis over-predicts the strain behavior at a location between two fasteners for applied stress below ~100 MPa. It is also noted that a reasonably good stress-strain correlation is observed for applied stress greater than ~100 MPa, implying that a more equal load distribution between two fasteners is achieved in the higher applied stress range. The percentage errors for both stress-strain correlations at the two different locations were initially between 8–30% margin (conservative), and when the midfastener issue described above is removed, the results lay in a range considered acceptable.

## VI. Displacement Analysis

Having validated the modeling technique by sheet strain evaluation, the model was used to predict joint displacements at the exposed sheet ends in the selected specimens. The displacements in simple lap joints, presented in Fig. 9 (countersunk fastened) and Fig. 10 (domehead-fastened) and subjected to their critical failure

**Table 1 Comparison of strain measurement with maximum applied stress of 150 MPa at $w = 12.5$ mm with respect to different element sizes**

| Element size, mm | Number of elements | Measurement, $\mu$str | Prediction, $\mu$str | Difference, % |
|---|---|---|---|---|
| 2.00 | 15394 | 685 | 545.3 | 20.4 |
| 1.50 | 21996 | 685 | 553.4 | 19.2 |
| 1.25 | 31716 | 685 | 575.8 | 15.9 |
| 1.00 | 45182 | 685 | 574.1 | 16.2 |

**Table 2 Comparison of strain measurement with minimum applied stress of −39 MPa at $w = 12.5$ mm with respect to different element sizes**

| Element size, mm | Number of elements | Measurement, $\mu$str | Prediction, $\mu$str | Difference, % |
|---|---|---|---|---|
| 2.00 | 15394 | −182 | −229.2 | 25.9 |
| 1.50 | 21996 | −182 | −227.9 | 25.2 |
| 1.25 | 31716 | −182 | −228.6 | 25.6 |
| 1.00 | 45182 | −182 | −226.8 | 24.6 |

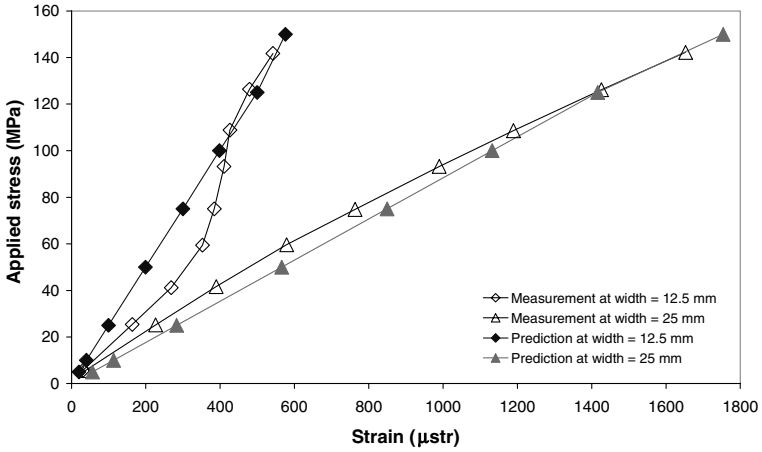


**Fig. 14 Model validation: influence of applied stress on strain distribution.**

stresses, 191 MPa and 169 MPa, respectively, were analyzed. In addition, a simple fatigue test on a domehead-fastened joint was performed to validate the finite element predictions of joint end deflection.

### A. Lap Joint (Countersunk)

Load transfer from one sheet to another occurs through both fastener shear and friction between faying surfaces. As a result, stress concentrations arise at the hole edge. Combining the effects of these stress raisers with secondary bending effects due to eccentricities in the joint, gives rise to complex three-dimensional stress distributions along the cross-sectional area near the hole edge, assisting development of fatigue cracks at these locations. This phenomenon has a detrimental effect on the fatigue life of a joint [33].

The opening-up of the exposed sheet ends, induced by the joint eccentricities as predicted by finite element analysis (see Fig. 15), will cause the coating system around this locus to deform, thus introducing additional strain in paint coatings. Under this complex strain cycling (both tension and compressive loads), a number of possible coating failures could occur, including coating surface microcracking that leads to through-thickness cracking or interfacial buckling delamination as discussed earlier. A full understanding of the displacement distribution at the sheet ends and the extent of structural damage caused by this displacement is therefore necessary for prediction and optimization of coating life.

Figure 16 shows the resultant displacement distribution (i.e., resultant of shear and out-of-plane displacements) along the width of specimen, i.e., from points A to B given in Fig. 15. The displacement calculated is between the point at the top corner of the upper sheet, and the point on the lower sheet where the upper sheet was originally in contact with the lower sheet, i.e., between points D and C in Fig. 15. The maximum displacement is found to occur between two fasteners since there is less fastener clamping and thus less shear friction at this location. The result also indicates that the effect of fastener clamping is a significant one, and will need to be factored into future analyses. Another important observation is that the out-of-plane displacement can contribute significantly in coating elongation due to the effect of joint eccentricity (it may be three to 5 times greater than the shear displacement). This effect causes rotation of the unloaded sheet end, and hence adds strain to the coated sealant at the sheet end. Future work will assess the effects of any additional substructure since this is expected to change the eccentricity, and lead to additional variation in displacement, depending on configuration.

### B. Generic Lap Joint (Dome-Head)

*1. Numerical Results*

Similar conclusions were reached from the finite element analysis of a simple lap joint fastened with domehead fasteners. The effect of secondary bending is significant, as can be seen in Fig. 17, and the bending stress is greatest at the top surface of the lower sheet, near the exposed sheet ends. Figure 18 presents the resultant displacement distribution between points D and C along the width of the specimen at exposed sheet ends, i.e., from point A to B in Fig. 17. Again, it is noted that sections between two adjacent fasteners experienced the greatest end deflection.

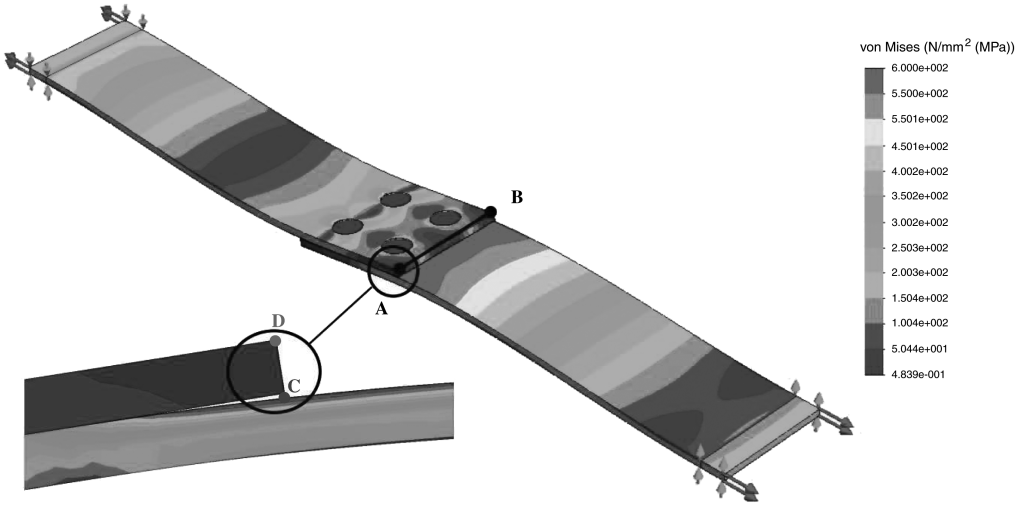


**Fig. 15 The von Mises stress distribution around overlap fastened section (countersunk fastener).**

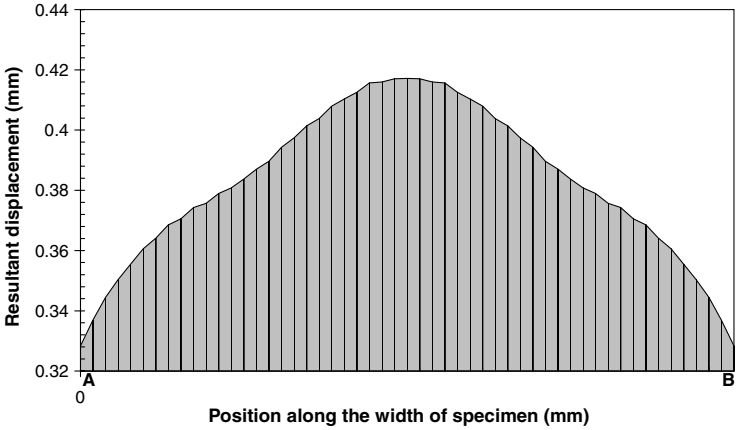


**Fig. 16 Resultant displacement distributions (between points C and D in Fig. 15) across the width of the countersunk-fastened specimen (along AB of Fig. 15).**

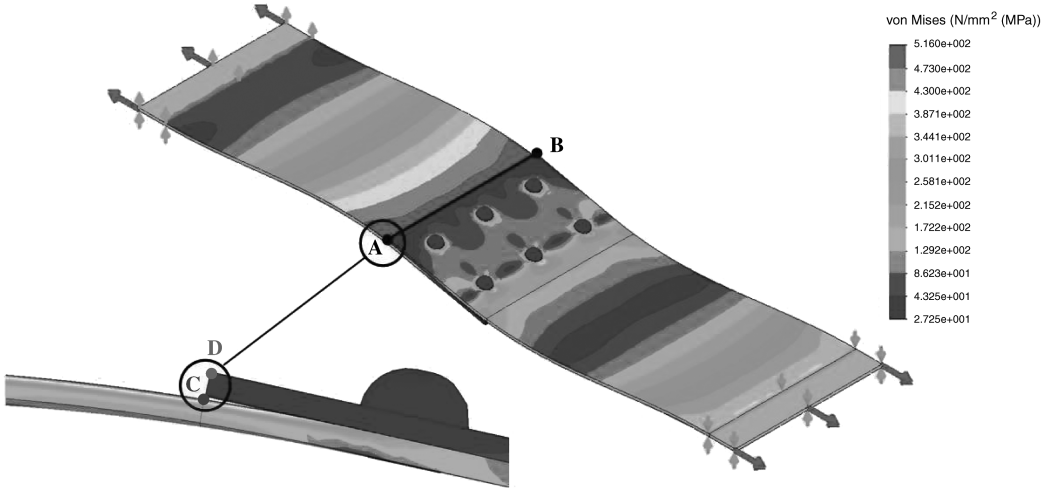


**Fig. 17 The von Mises stress distribution around overlap fastened section (domehead fastener).**

A simple fatigue test on this domehead-fastened joint was designed to measure the displacements, both shear and out-of-plane components for comparison with the prediction. The following section describes the experimental setup and procedures.

### 2. *Experimental Setup and Results*

The fatigue test was carried out using a 250 kN MTS servo-controlled hydraulic testing machine under constant amplitude loading and ambient laboratory conditions, see Fig. 19. The test specimen was loaded in tension to give a remote stress of 169 MPa. Maximum and minimum loads used were 9.8 and 0.98 kN, respectively, giving a stress ratio of 0.1 at a frequency of 1 Hz. Ruler scales with an interval of $1/6$ in. ($\sim$0.397 mm) were attached along the exposed edge of the sheet, so that any displacements around the sheet ends could be measured.

A digital camera was mounted facing the exposed sheet front of the specimen to record shear movements. The scale was attached at a point between two adjacent fasteners, where the maximum shear displacement was predicted. Experimental limitations meant that the

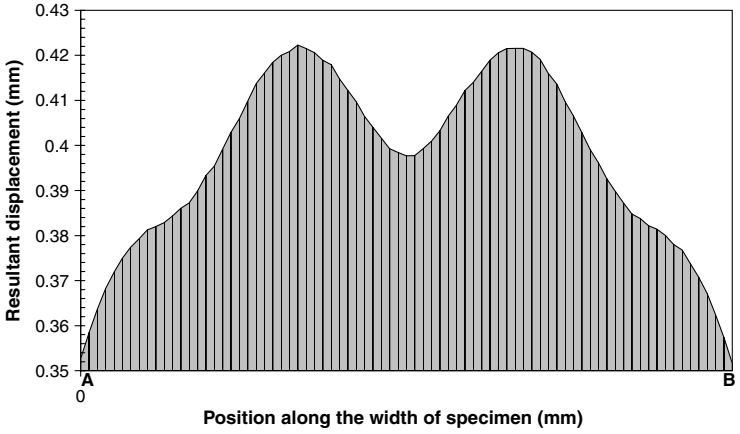


**Fig. 18 Resultant displacement distributions (between points C and D in Fig. 17) across the width of domehead-fastened specimen (along AB of Fig. 17).**

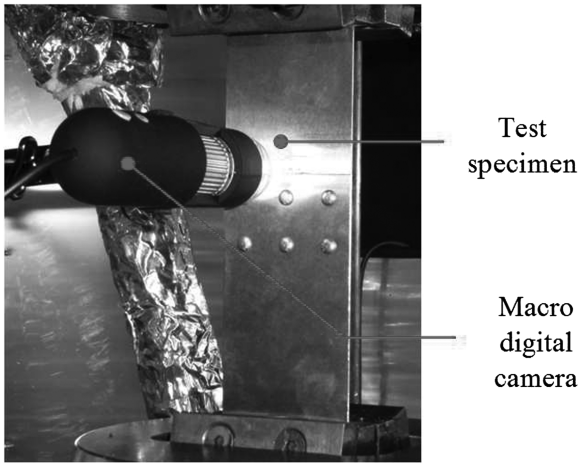


**Fig. 19 Experimental apparatus setup.**

shear displacement that could be measured visibly was the relative displacement between exposed surfaces of top and bottom sheets. A video recording was made throughout the cycling process for 20 cycles. A second fatigue test with similar procedures was carried out to record the out-of-plane movements at the sheet edge. In this instance, the camera was mounted facing the specimen edge. Here the measured out-of-plane displacement was the relative displacement between faying and exposed surfaces of top and bottom sheets, respectively, (i.e., change of displacement between point C and D in Fig. 20).

The test confirmed the occurrence of shear movements and opening up of sheet ends, as predicted, at an applied load of 9.8 kN (see Fig. 20). Image processing and measurement was performed using ImageJ to measure the values of both shear and out-of-plane displacement. The displacements were calibrated and measured using picture density standards. The tests were run for 20 cycles, so 20 values for each displacement (i.e., shear and out-of-plane) were collected. The mean values of these samples are given in Table 3, and were 0.199 and 0.236 mm for shear and out-of-plane displacements, respectively.

### 3. *Comparison of Experimental and Predicted Results*

The correlations were reasonably good, with an error margin between 29–34% for shear displacement, and 20–29% error margin for out-of-plane displacements. In both cases, the predicted values are higher than experimentally measured values, i.e., the prediction was conservative.

The differences between prediction and experiment observed are likely to be caused by the finite element parameters adopted (specific assumed values likely to need attention in future work include clamping force, frictional coefficients at contacting surfaces, and fastener constraints) as well as any experimental measurement errors [59]. Future work involves refining the model, and validating the finite element parameters which involve fastener assumptions, and will use additional experimental techniques, such as laser speckle interferometry and noncontacting video extensometer, to provide more detailed measurement of joint movements.

## VII. Discussion: Impact on Coating Degradation

The analysis shows that sheet ends of lap joints tend to open up during cyclic loading, and that secondary bending plays a significant role in this effect due to the joint geometric eccentricities. Local deformation/bending will therefore occur in any coating system around this location. The detrimental effect on coatings is therefore likely to vary depending on several joint design parameters, namely applied tensile loads and the dimensions of the joint (such as sheet thickness, fastener pitch, fastener spacing, etc.) [33].

The joint considered is a domehead-fastened lap joint as presented earlier in Fig. 10. In real structural joints, a fillet of sealant coat or adhesive, which is squeezed out under pressure while the joint is being manufactured, is often applied, as shown in Fig. 21. Assuming a 45° bead of sealant and coating covering the exposed sheet ends, the effective length of the surface of the coating, i.e., the length of the applied topcoat, is denoted here as $l^*$ (i.e., along line D to E in Fig. 21). The finite element results provide the change of this effective length $l^*$, i.e., the displacement between points D and E, at a location between fasteners, under tensile loading. The resultant displacement along $l^*$ is calculated to be $\Delta l^* = 0.315$ mm. Note that this calculated value is smaller than the previous predicted values for displacements of points C to D given earlier in Fig. 18, due to the effect of joint eccentricity which causes rotation at the unloaded sheet ends, such as at point D. To ensure the representativeness of the analysis, the strain of sealant/coating bead was estimated from the change of the effective length $l^*$ (i.e., displacement along points D to E); while the displacement of points C and D, as discussed in Sec. VI, was used for the initial joint displacement validation because of the convenience in measuring the displacement along points C and D during the test.

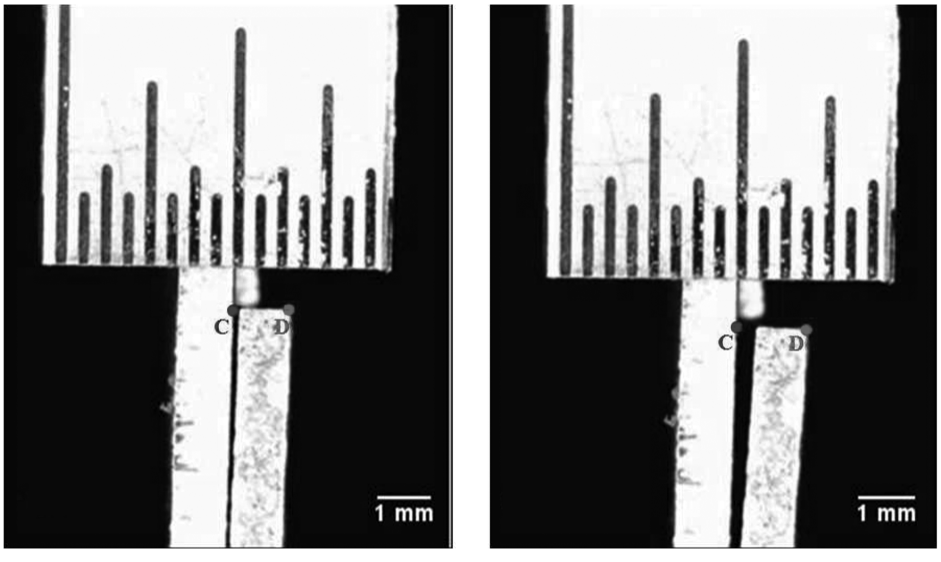


a) b)

**Fig. 20 Experimental observations (out-of-plane displacement) during fatigue test: a) before testing, and b) at approximately 9.8 kN (critical) applied load.**

**Table 3 Experimental measurements (sample mean)**

| Location | Relative displacement, mm |
|---|---|
| Sheet front (between adjacent fasteners) | 0.199 |
| Sheet edge (edge of exposed sheet) | 0.236 |

Based on the estimated $\Delta l^*$ value, the strain in the surface of the coatings was calculated to be 21.9%. Note that this value corresponds to applied loading greater than the maximum service load. A value about 2/3 of this [60], i.e., 14% is therefore a better representation of maximum strain in service, assuming linear behavior. The value of this concentrated strain is substantially higher than normally experienced on, say, a flat sheet in the middle of the wing (where the strain experienced is expected to be closer to 1%).

The airframe often experiences significant temperature variation during its service lifetime, particularly for high-performance military aircraft. During climb, the skin temperature drops initially due to the exposure to decreasing ambient air temperature. However, as the speed of aircraft increases the skin temperature can increase dramatically due to the effect of aerodynamic heating; in a military aircraft, skin temperatures over 100°C may be achieved. During descent, the reverse process occurs. The thermal expansion mismatch between coating system and substrate contributes additional stress in the aircraft paint coatings, and this thermal strain $\varepsilon_{\text{th}}$ may also contribute to coating degradation by adding to the mechanical loading, so the total strain in the sealant/paint bead could be much higher than the calculated service strain of 14% $\varepsilon_m$. Thermal strain will be considered in future investigations, as will an additional parameter: the hygroscopic strain $\varepsilon_h$ arising in the paint coating due to absorption and desorption of water as a result of variation in the relative humidity.

Hegedus et al. [64] noted that although epoxy primers have relatively high tensile strength (>17 MPa), they have poor elongation (<10%) at break. A service strain value of 14% could therefore easily exceed the critical strain-to-failure for such a material. Our primary focus is the fracture critical polyurethane topcoat which is exposed to a wider range of environmental conditions, and, if it cracks, allows moisture ingress. The potential failure mode along $l^*$ is essentially tensile cracking in the polyurethane topcoat, with microcracks initiating from surface irregularities, microvoids or even maintenance-induced or impact-induced scratches. Newly applied polyurethane topcoat has much higher strain tolerance than its underlying epoxy primer, i.e., exhibits elongation at break greater than 100% and higher tensile strength [39]. Its fracture toughness $K_c$ has been determined to be approximately 1 MPa $\text{m}^{1/2}$ [65]. When the in-plane stress is applied to preexisting defects, and this value of fracture toughness is reached, the preexisting defects will propagate, leading to coating failure.

Although fresh polyurethane topcoat is flexible and will tolerate the calculated strain at sheet ends, aging of the coating under the influence of ultraviolet radiation and thermal cycling will degrade its mechanical properties. To scope this effect, we have used Eq. (1) to estimate the degradation rate of polyurethane topcoat considering two important factors, namely 1) the weathering exposure time and 2) the change of its surface topography (i.e., size of the surface defect). Indeed, past research [66,67] has shown that the mechanical integrity and the lifetime of the topcoat depend crucially on these two factors. Here Eq. (1) can be rewritten by relating critical strain to the Young's modulus of coating and surface crack size:

$$\varepsilon_{\text{cr}} = \frac{K_c(1-\upsilon_c)}{\beta E\sqrt{\pi a}} \tag{5}$$

**Table 4 Mechanical properties of polyurethane, taken from [39,67]**

| Exposure period, week | Modulus by nanoindentation, GPa | Average size of surface defect, nm |
|---|---|---|
| 0 | $1.60 \pm 0.27$ | 90 |
| 1 | $2.00 \pm 0.15$ | |
| 2 | $2.30 \pm 0.35$ | 195 |
| 4 | $2.40 \pm 0.30$ | |
| 5 | | 498 |
| 6 | $2.94 \pm 0.50$ | |
| 8 | $3.47 \pm 0.90$ | |
| 9 | | 1327 |
| 13 | | 1605 |

Using the modulus data given in Table 4, in Eq. (5), Fig. 22 shows the "moving average" of the polyurethane strain degradation curve given in a function of accelerated weathering exposure period in the test chamber. Here, $K_c$ is taken to be 1 MPa $\text{m}^{1/2}$ and $\beta$ is equal to one [65]. From this, admittedly unsophisticated, model, we can see that the polyurethane material's elongation-at-break decays significantly with increasing exposure time, indicating weakening of the polyurethane material strength due to weathering/aging.

For a fresh paint (i.e., when the exposure time is equal to zero), the fracture strain is estimated as 65%. Since the local service strain at the 45° sealant/coating bead is calculated to be of the order of 14%, there should be no adverse effect on the mechanical integrity of fresh paint. However, from Fig. 22, the fracture strain drops below 14% level after six weeks of accelerated weathering exposure, suggesting that premature paint failure could occur at this location should a service strain of 14% be applied. For the coating to remain effective, it is critical to ensure that the strength of the coating remains above the in-service strain levels, and part of an ongoing testing program are to validate the paint coating durability at this applied strain level, subjected to different accelerated weathering exposure time.

The lap joint with countersunk fasteners as shown in Fig. 9 displays an end-bead service strain of 10% as a reasonable estimate for a maximum service condition. Using the same approach, this concentrated strain would appear capable of causing failure in aged paint after several weeks of accelerated weathering exposure. The differences in the estimated concentrated strain values for the joints results simply from the different sheet materials used, strength and type of fastener used, joint types, etc.

These results suggest that the "mechanical" part of a thermo-mechanical environmental history is significant for coating durability. Furthermore, secondary bending at mechanical joints seems to

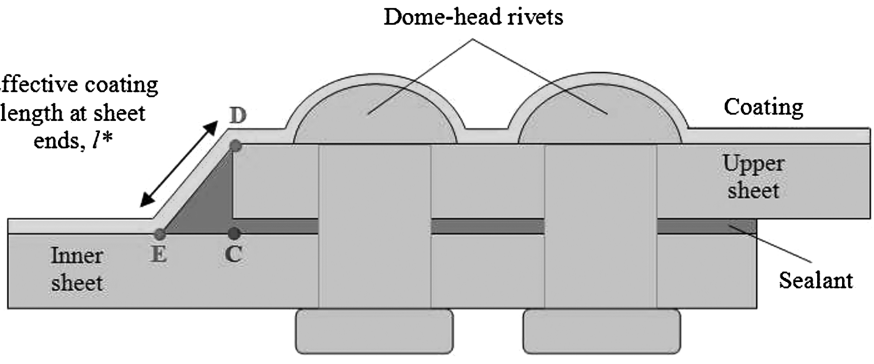


**Fig. 21 Effective length of coatings covering joint sheet ends.**

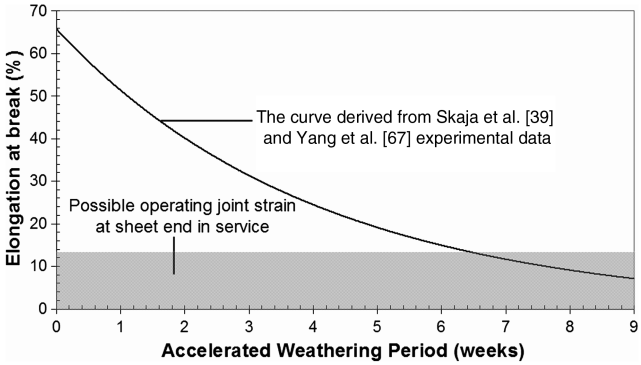


**Fig. 22 Fatigue strength of polyurethane topcoat against weathering exposure period in the test chamber.**

be a particularly important factor; this factor will impart significant variability since different joint cases will exhibit a range of secondary bending behaviors.

Several research issues arise when considering how to translate the results into a usable representation of service history, viz:

1) The degradation probably cannot be determined simply by adding a strain to a coating exposure, since the sequence of loading throughout service life is likely to be important.

2) Application of high service load to a fresh coating may produce little physical damage, compared with application of the same load later in the coating life.

3) It may be that a very high load early in life might enhance some forms of microstructural degradation, particularly if that loading leads to early cracking and moisture ingress.

4) The residual strength of the coating will reduce progressively through the service life, but the actual failure point will be determined by a combination of the decaying residual strength and the level of loading applied, and this will lead to variability in the service life of the coating.

5) Clearly there is need to evaluate a range of thermomechanical environmental profiles, for use in both experimental evaluation of coatings, and as a base for prediction of coating durability.

## VIII. Conclusions

This research has highlighted the extent to which displacements in aircraft joints might be a factor influencing the longevity of aircraft protective coatings such as paints and sealants. Finite element modeling on two lap joints fastened with countersunk and domehead fasteners was used to predict the joint end deflection at exposed sheet ends, and the predictions were validated using fatigue tests. The results indicate:

1) The displacement predicted and observed represents coating strains of the order of 10 and 14%, and these strains are a factor which should be incorporated in development of a *thermomechanical* environmental history for coating tests and for prediction of coating durability. Both coating degradation and coating failure conditions are likely to be affected by these complex and repeated in-service strain cycles.

2) Numerical modeling and fatigue tests were performed for two simple lap joints. These numerical and experimental results showed that, for a two-row mechanically fastened lap joint, the maximum joint end deflection is greater than 300 micrometers, of which a substantial fraction derives from secondary bending. Overall, secondary bending was observed to be a very significant factor driving joint displacement. Load path eccentricities cause the exposed sheet ends to deflect and contribute substantially to the service strain on coatings.

3) Maximum joint end deflection was predicted and observed to occur at sheet ends between two adjacent fasteners since these regions are more remote from the structural influence of fastener shear.

4) This initial work has focused on sheet ends, but other potential coating failure locations such as fastener head/countersink regions, are expected to be important.

5) Incorporating mechanical effects into the overall environmental history raises a number of issues which will need to be addressed to develop useful representations of thermomechanical service histories. A major issue will be the variability in strain application, and how that interacts with the progressive degradation of the coating. A particular issue is the way in which high loads might 1) enhance early degradation of coatings, and 2) dominate the timing of failure of a degraded coating later in life.

This paper has illustrated the importance of joint displacements on an overlying coating intended to provide corrosion protection. Future work will consider additional locations and other aspects of the thermomechanical history effect, such as load sequence effect, cumulative damage estimation, interfacial adhesion strength, and residual stress, all of which may play significant roles in influencing the longevity of aircraft protective coatings.

## Acknowledgments

The authors would like to acknowledge with gratitude financial support from the Defence Materials Technology Centre, Ltd. In addition, thanks are due to Don Savvides, Patrick Wilkins, and Peter Tkatchyk (RMIT) for their assistance in preparing test specimens and setting up experimental apparatus. Useful discussions with Bruce Crawford of the Defence Science and Technology Organisation are greatly appreciated.

## References

[1] Simpson, D. L., and Brooks, C. L., "Tailoring the Structural Integrity Process to Meet the Challenges of Aging Aircraft," *International Journal of Fatigue*, Vol. 21, No. 1, 1999, pp. 1–14. doi:10.1016/S0142-1123(99)00052-3

[2] Clark, G., and Jackson, P., "Structural Integrity and Damage Type in Military Aircraft," *Fatigue and Fracture of Engineering Materials and Structures*, Vol. 33, No. 11, 2010, pp. 752–764. doi:10.1111/j.1460-2695.2010.01486.x

[3] "AGARD Corrosion Handbook Volume 1, Aircraft Corrosion: Causes and Case Histories," AGARD AG-278, 1985.

[4] Cole, G. K., Clark, G., and Sharp, P. K., "The Implications of Corrosion with Respect to Aircraft Structural Integrity," DSTO Aeronautical and Maritime Research Laboratory, Melbourne, Australia, 1997.

[5] Kinzie, R., and Cooke, G., "Corrosion in USAF aging aircraft fleets," *Fatigue in the Presence of Corrosion*, RTO MP-18, Corfu, Greece, 1998.

[6] Urban, M. R., "Analysis of the Fatigue Life of Riveted Sheet Metal Helicopter Airframe Joints," *International Journal of Fatigue*, Vol. 25, Nos. 9–11, 2003, pp. 1013–1026. doi:10.1016/j.ijfatigue.2003.08.003

[7] Bellinger, N. C., Komorowski, J. P., and Gould, R. W., "Corrosion Pillowing in Aircraft Fuselage Lap Joints," *Journal of Aircraft*, Vol. 44, No. 3, 2007, pp. 758–763. doi:10.2514/1.18589

[8] "Aloha Airlines, Flight 243, Boeing 737-200, N73711, Near Maui, Hawaii, April 28, 1988," National Transportation Safety Board, NTSB/AAR-89/03, Washington, D.C., 1989.

[9] Furuta, S., Terada, H., and Sashikuma, H., "Fatigue Strength of Fuselage Joint Structures Under Ambient and Corrosive Environment," *ICAF'97: Fatigue in New and Aging Aircraft*, EMAS Publishing, Melbourne, Australia, 1997, pp. 231–249.

[10] Hoeppner, D. W., Grimes, L., Hoeppner, A., Ledesma, J., Mills, T., and Shah, A., "Corrosion and Fretting as Critical Aviation Safety Issues, Estimation, Enhancement and Control of Aircraft Fatigue Performance," *Proceedings of the 18th Symposium of the International Committee on Aeronautical Fatigue*, EMAS Publishing, Melbourne, Australia, 1995, pp. 87–106.

[11] Campbell, G. S., and Lahey, R., "A Survey of Serious Aircraft Accidents Involving Fatigue Fracture," *International Journal of Fatigue*, Vol. 6, No. 1, 1984, pp. 25–30. doi:10.1016/0142-1123(84)90005-7

[12] Clark, G., *Corrosion and the Management of Structural Integrity*, EMAS, Melbourne, Australia, 1999.

[13] Smith, C. J. E., Higgs, M. S., and Baldwin, K. R., "Advances in Protective Coatings and their Application to Ageing Aircraft," *The RTO*

*AVT Workshop on New Metallic Materials for the Structure of Aging Aircraft*, Canada Communications Group, Inc., Hull, Québec, Canada, 1999.

[14] Bache, M. R., Ward, A. R., Evans, W. J., Spence, S. H., Williams, N. M., Stonham, A. J., Hay, D., Urbani, C., Crawford, B. R., Loader, C., and Clark, G., "Effects of Mean Stress and Corrosion Pitting on Fatigue in an Aerospace Aluminium Alloy," *Fatigue and Durability Assessment of Materials, Components & Structures—FATIGUE 2003*, Engineering Integrity Society, Sheffield, 2003, pp. 57–64.

[15] Scholes, F. H., Furman, S. A., Hughes, A. E., and Markley, T. A., "Corrosion in Artificial Defects. I: Development of Corrosion," *Corrosion Science*, Vol. 48, No. 7, 2006, pp. 1812–1826. doi:10.1016/j.corsci.2005.05.050

[16] Kim, S. R., and Nairn, J. A., "Fracture Mechanics Analysis of Coating/Substrate Systems Part I: Analysis of Tensile and Bending Experiments," *Engineering Fracture Mechanics*, Vol. 65, No. 5, 2000, pp. 537–593. doi: 10.1016/S0013-7944(99)00141-1

[17] Miller, R., Seeliger, G. G., and Boggs, W. A., "Protective Systems for Fastener Areas of Carrier-Based Naval Aircraft," *Materials Performance*, Vol. 14, No. 8, 1975, pp. 28–32.

[18] "Aging of U.S. Air Force Aircraft: Final Report," Committee on Aging of U.S. Air Force Aircraft, Commission on Engineering and Technical Systems and National Research Council, National Academy Press Rept. No. NMAB-488-2, Washington, D.C., 1997.

[19] Silva, L. F. M., Goncalves, J. P. M., Oliveira, F. M. F., and de Castro, P. M. S. T., "Multiple-Site Damage in Riveted Lap-Joints: Experimental Simulation and Finite Element Prediction," *International Journal of Fatigue*, Vol. 22, No. 4, 2000, pp. 319–338. doi:10.1016/S0142-1123(99)00129-2

[20] Starikov, R., and Schön, J., "Quasi-Static Behavior of Composite Joints with Countersunk Composite and Metal Fasteners," *Composites, Part B: Engineering*, Vol. 32, No. 5, 2001, pp. 401–411. doi:10.1016/S1359-8368(01)00013-0

[21] Starikov, R., and Schön, J., "Quasi-Static Behavior of Composite Joints with Protruding-Head Bolts," *Composite Structures*, Vol. 51, No. 4, 2001, pp. 411–425. doi:10.1016/S0263-8223(00)00157-4

[22] Starikov, R., "Fatigue Behavior of Mechanically Fastened Aluminium Joints Tested in Spectrum Loading," *International Journal of Fatigue*, Vol. 26, No. 10, 2004, pp. 1115–1127. doi:10.1016/j.ijfatigue.2004.03.006

[23] Rettew, H. F., and Thumin, C., "Tests on Riveted Joints in Sheet Duralumin," NACA TN165, 1924.

[24] Fawaz, S. A., and Schijve, J., "Fatigue Crack Growth Prediction in Riveted Joints," NASA CP-1999-208982, 1999.

[25] Shin, Y. S., Iverson, J. C., and Kim, K. S., "Experimental Studies on Damping Characteristics of Bolted Joints for Paltes and Shells," *ASME Pressure Vessels and Piping Conference*, Vol. 113, American Society of Mechanical Engineers, Fairfield, NJ, 1991, pp. 402–408.

[26] Gresnigt, A. M., and Steenhuis, C. M., "Stiffness of Lap Joints with Preloaded Bolts," *Proceedings of the NATO ARW*, Kluwer Academic Publishers, Dordrecht, The Netherlands, 2000.

[27] Tate, M., "Preliminary Investigation of the Loads Carried by Individual Bolts in Bolted Joints," NACA TN1051, 1946.

[28] Eastaugh, G. F., Simpson, D. L., Straznicky, P. V., and Wakeman, R. B., "A Special Uniaxial Coupon Test Specimen for the Simulation of Multiple Site Fatigue Crack Growth and Link-Up in Fuselage Skin Splices," NASA 96N24261, 1995.

[29] Piascik, R. S., Willard, S. A., and Miller, M., "The Characterization of Widespread Fatigue Damage in Fuselage," NASA 95N14920, 1994.

[30] Sharp, M. L., Nordmark, G. E., and Menzemer, C. C., *Fatigue Design of Aluminum Components and Structures*, McGraw–Hill, New York, 1996.

[31] Niu, C. Y., *Airframe Structural Design. Practical Design Information and Data on Aircraft Structures*, Hong Kong Conmilit Press Ltd, Hong Kong, 1999.

[32] Park, C. Y., and Grandt, A. F., "A Proposed Fatigue Test Protocol for Generic Mechanical Joints," *Engineering Failure Analysis*, Vol. 13, No. 1, 2006, pp. 136–154. doi:10.1016/j.engfailanal.2004.10.013

[33] Schijve, J., Campoli, G., and Monaco, A., "Fatigue of Structures and Secondary Bending in Structural Elements," *International Journal of Fatigue*, Vol. 31, No. 7, 2009, pp. 1111–1123. doi:10.1016/j.ijfatigue.2009.01.009

[34] Finney, J. M., and Evans, R. L., "Extending the Fatigue Life of Multi-Layer Metal Joints," *Fatigue & Fracture Engineering Materials and Structures*, Vol. 18, No. 11, 1995, pp. 1231–1247. doi: 10.1111/j.1460-2695.1995.tb00851.x

[35] Schutz, D., and Lowak, H., "The Effect of Secondary Bending on the Fatigue Strength of Joints," Laboratorium fur Betriebsfetigkeit Rept. FB-113, 1974.

[36] Farrier, L. M., and Szaruga, S. L., "Sample Preparation and Characterization of Artificially Aged Aircraft Coatings for Microstructural Analysis," *Materials Characterization*, Vol. 55, No. 3, 2005, pp. 179–189. doi:10.1016/j.matchar.2005.04.009

[37] Feldman, D., "Polymer Weathering: Photo-Oxidation," *Journal of Polymers and the Environment*, Vol. 10, No. 4, 2002, pp. 163–173. doi:10.1023/A:1021148205366

[38] Ranby, B., and Rabek, J. F., *Photodegradation, Photo-Oxidation and Photostabilisation of Polymers, Principles and Application*, Wiley-Interscience, New York, 1975.

[39] Skaja, A., Fernando, D., and Croll, S., "Mechanical Property Changes and Degradation During Accelerated Weathering of Polyester-Urethane Coatings," *Journal of Coatings Technology and Research*, Vol. 3, No. 1, 2006, pp. 41–51. doi: 10.1007/s11998-006-0004-7

[40] Kramb, V. A., Hoffman, J. P., and Johnson, J. A., "Characterization of Weathering Degradation in Aircrft Polymeric Coatings Using NDE Imaging Techniques," *American Institute of Physics Conference Proceedings. Review of Progress in Quantitative Nondestructive Evaluation*, Vol. 657, No. 1, 2003, pp. 1111–1118. doi:10.1063/1.1570257

[41] Guo, X., Michaels, C. A., Drzal, P. L., Jasmin, J., Martin, D., Nguyen, T., and Martin, J. W., "Probing Photodegradation Beneath the Surface: A Depth Profiling Study of UV-Degraded Polymeric Coating with Microchemical Imaging and Nanoindentation," *Journal of Coatings Technology and Research*, Vol. 4, No. 4, 2007, pp. 389–399. doi:10.1007/s11998-007-9052-x

[42] Bondzic, S., Hodgkin, J., Krstina, J., and Mardel, J., "Chemistry of Thermal Aging in Aerospace Epoxy Composites," *Journal of Applied Polymer Science*, Vol. 100, No. 3, 2006, pp. 2210–2219. doi:10.1002/app.23692

[43] Thompson, D. G., Osborn, J. C., Kober, E. M., and Schoonover, J. R., "Effects of Hydrolysis-Induced Molecular Weight Changes on the Phase Separation of a Polyester Polyurethane," *Polymer Degradation and Stability*, Vol. 91, No. 12, 2006, pp. 3360–3370. doi:10.1016/j.polymdegradstab.2006.05.019

[44] Yang, X. F., Vang, C., Tallman, D. E., Bierwagen, G. P., Croll, S. G., and Rohlik, S., "Weathering Degradation of a Polyurethane Coating," *Polymer Degradation and Stability*, Vol. 74, No. 2, 2001, pp. 341–351. doi:10.1016/S0141-3910(01)00166-5

[45] Yang, X. F., Tallman, D. E., Bierwagen, G. P., Croll, S. G., and Rohlik, S., "Blistering and Degradation of Polyurethane Coatings Under Different Accelerated Weathering Tests," *Polymer degradation and stability*, Vol. 77, No. 1, 2002, pp. 103–109. doi:10.1016/S0141-3910(02)00085-X

[46] Tangestanian, P., Papini, M., and Spelt, J. K., "Starch Media Blast Cleaning of Artificially Aged Paint Films," *Wear*, Vol. 248, Nos. 1–2, 2001, pp. 128–139. doi:10.1016/S0043-1648(00)00552-4

[47] White, J. R., and Turnbull, A., "Weathering of Polymers: Mechanisms of Degradation and Stabilization, Testing Strategies and Modelling," *Journal of Materials Science*, Vol. 29, No. 3, 1994, pp. 584–613. doi:10.1007/BF00445969

[48] Terselius, B., Gedde, U. W., and Jansson, J. F., "Mechano-Chemical Phenomena in Polymers," *Failure of Plastics*, SPE Hanser, Munich, 1986, pp. 273–286.

[49] Popov, A. A., Rapoport, N., and Zaikov, G., *Oxidation of Stressed Polymers*, Gordon and Breach Science Publishers, New York, 1991.

[50] Czerný, J., "Thermo-Oxidative and Photo-Oxidative Aging of Polypropylene Under Simultaneous Tensile Stress," *Journal of Applied Polymer Science*, Vol. 16, No. 10, 1972, pp. 2623–2632. doi:10.1002/app.1972.070161015

[51] Strawbridge, A., and Evans, H. E., "Mechanical Failure of Thin Brittle Coatings," *Engineering Failure Analysis*, Vol. 2, No. 2, 1995, pp. 85–103. doi:10.1016/1350-6307(95)00014-H

[52] Grosskreutz, J. C., and McNeil, M. B., "The Fracture of Surface Coatings on a Strained Substrate," *Journal of Applied Physics*, Vol. 40, No. 1, 1969, pp. 355–359. doi:10.1063/1.1657059

[53] Nair, J. A., and Kim, S. R., "A Fracture Mechanics Analysis of Multiple Cracking in Coatings," *Engineering Fracture Mechanics*, Vol. 42, No. 1, 1992, pp. 195–208. doi:10.1016/0013-7944(92)90291-L

[54] Evans, A. G., and Hutchison, J. W., "On the Mechanics of Delamination and Spalling in Compressed Films," *International Journal of Solids and Structures*, Vol. 20, No. 5, 1984, pp. 455–466. doi:10.1016/0020-7683(84)90012-X

[55] Thouless, M. D., "Some Mechanics for the Adhesion of Thin Films," *Thin Solid Films*, Vol. 181, Nos. 1–2, 1989, pp. 397–406. doi:10.1016/0040-6090(89)90508-7

[56] Hutchinson, J. W., He, M. Y., and Evans, A. G., "The Influence of Imperfections on the Nucleation and Propagation of Buckling Driven Delaminations," *Journal of the Mechanics and Physics of Solids*, Vol. 48, No. 4, 2000, pp. 709–734. doi:10.1016/S0022-5096(99)00050-2

[57] Evans, A. G., Drory, M. D., and Hu, M. S., "The Cracking and Decohesion of Thin Films," *Journal of Materials Research*, Vol. 3, No. 5, 1988, pp. 1043–1049. doi:10.1557/JMR.1988.1043

[58] Evans, H. E., and Lobb, R. C., "Conditions for the Initiation of Oxide-Scale Cracking and Spallation," *Corrosion Science*, Vol. 24, No. 3, 1984, pp. 209–222. doi:10.1016/0010-938X(84)90051-9

[59] Tiong, U. H., and Clark, G., "The Structural Environment as a Factor Affecting Coating Failure in Aircraft Joints," *Procedia Engineering*, Vol. 2, No. 1, 2010, pp. 1393–1401. doi:10.1016/j.proeng.2010.03.151

[60] Tiong, U. H., and Clark, G., "Influence of Mechanical Loading on Failure of Aircraft Protective Coatings," *Materials Science Forum*, Vols. 654–656, 2010, pp. 2503–2506. doi:10.4028/www.scientific.net/MSF.654-656.2503

[61] "Hi-Lok Product Specification 342, 100 Flush Shear Head, Alloy Steel," Hi-Shear Corporation, Torrance, CA, 1992.

[62] Atre, A., and Johnson, W. S., "Analysis of the Effects of Interference and Sealant on Riveted Lap Joints," *Journal of Aircraft*, Vol. 44, No. 2, 2007, pp. 353–364. doi: 10.2514/1.18320

[63] Starikov, R., and Schön, J., "Local Fatigue Behavior of CFRP Bolted Joints," *Composites Science and Technology*, Vol. 62, No. 2, 2002, pp. 243–253. doi:10.1016/S0266-3538(01)00200-7

[64] Hegedus, C. R., Spadafora, S. J., Pulley, D. F., Eng, A. T., and Hirst, D. J., *Paint and Coating Testing Manual*, Ch. Aerospace and Aircraft Coatings, ASTM International, West Conshohocken, PA, 1995.

[65] Ni, H., Daum, J. L., and Soucek, M. D., "Cycloaliphatic Polyester Based High Solids Polyurethane Coatings: I. The Effects Of Difunctional Alcohols," *Journal of Coatings Technology*, Vol. 74, No. 5, 2002, pp. 49–56. doi:10.1007/BF02697983

[66] Schmid, E. V., *Exterior Durability of Organic Coatings*, FMJ International, Surrey, England, 1988.

[67] Yang, X. F., Li, J., Croll, S., Tallman, D. E., and Bierwagen, G. P., "Degradation of Low Gloss Polyurethane Aircraft Coatings Under UV and Prohesion Alternating Exposures," *Polymer degradation and stability*, Vol. 80, No. 1, 2003, pp. 51–58. doi:10.1016/S0141-3910(02)00382-8

[68] Tiong, U. H., and Clark, G., "Critical Strain Performance of Coating Systems at Aircraft Joints," *27th International Congress of the Aeronautical Sciences*, Nice, France, 2010.